Optimization of the Loop-Coupled Log-Periodic Antenna

CLIVE R. OAKES AND KEITH G. BALMAIN

Abstract—**Varying the spacing between the transposed transmission line feeder and the radiating elements of the loop-coupled antenna is investigated experimentally using far-field swept-frequency techniques. An optimum spacing is found in the sense that anomalous frequency performance is minimized. A theory using dispersion relationships is developed and used to explain some of the experimental phenomena observed.**

I. Introduction

THE ANTENNA (Fig. 1) consists of two inductively coupled log-periodic structures [1], one being the array of unbroken dipoles and the other being the transposed transmission line. The investigation to be described uses far-field swept-frequency measurement techniques and reveals that, unless the spacing t is optimum, anomalous behaviour occurs. The use of a theoretical modified dispersion diagram aids in the interpretation of observed truncation effects and provides insight into the phase-matching aspect of the optimization procedure.

II. Experimental Data

The measurements were taken in an anechoic chamber using for a source a standard log-periodic dipole antenna driven by a sweep generator. The source antenna was optimized as described in [2] to be free of frequency-dependent anomalies. The technique used is to aim the test antenna at the source antenna, measure the far-field received signal over a frequency sweep, rotate the antenna an angle ϕ in the E plane or an angle ψ in the H plane, take the frequency response again, and repeat until a family of curves is obtained (many examples are shown in [3]). Because the gain and pattern of an ideal log-periodic antenna are fixed with frequency, and the transmission formula [4] indicates received power proportional to λ^2, the family of curves just described should consist of approximately parallel straight lines with a -6 dB/octave slope on a log-frequency scale.

The generator sweep range was from 0.5 GHz to 1.0 GHz; however, all graphs and formulas use F which is the frequency normalized to the half-wavelength frequency (0.5 GHz) of the longest element. A germanium point-contact diode was placed across the feed-point of the loop-coupled antenna and the demodulated audio signal was taken out of the back termination across a

Manuscript received April 18, 1972; revised September 19, 1972. This work was supported in part by the Defence Research Board of Canada under Grant 9510-70 and in part by the National Research Council of Canada under Grant A-4140.

The authors are with the Department of Electrical Engineering, University of Toronto, Toronto, Ont., Canada M5S 1A4.

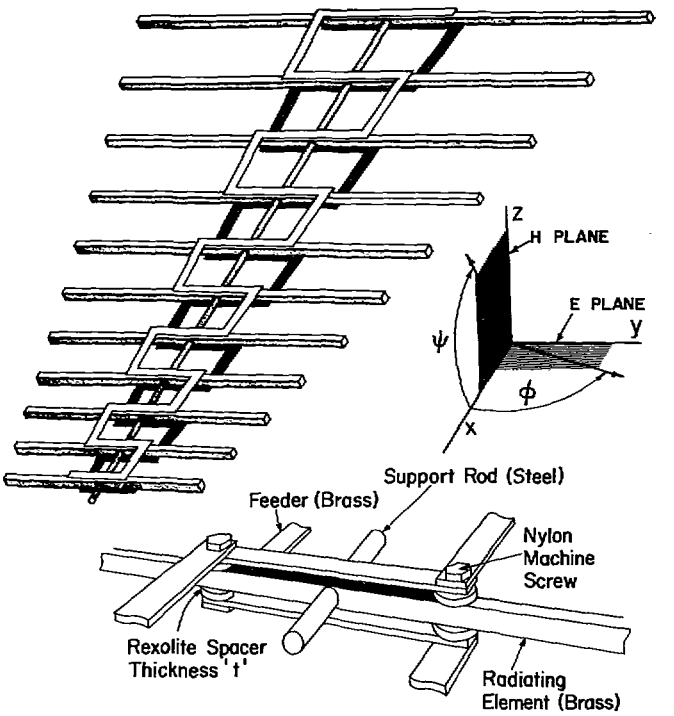

Fig. 1. Loop-coupled log-periodic antenna. Feed terminals are at small end of array and large end can be terminated with short circuit, open circuit, or resistive load. Elements are $\frac{3}{16}$ in square brass rods.

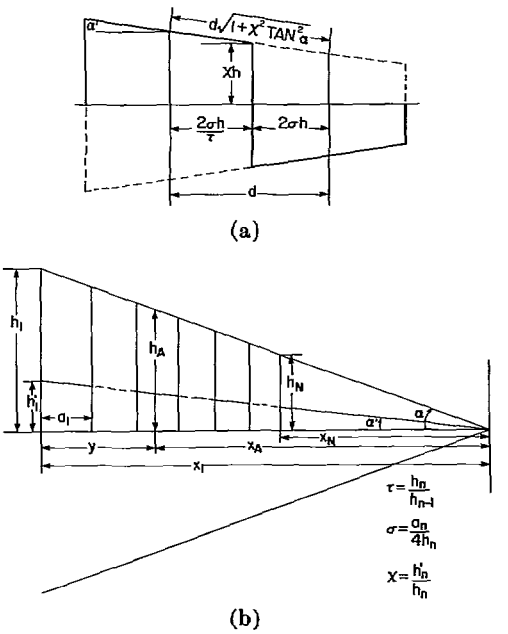

Fig. 2. (a) Definition of cell of transposed transmission line. (b) Definition of log-periodic parameters τ, σ, and χ.

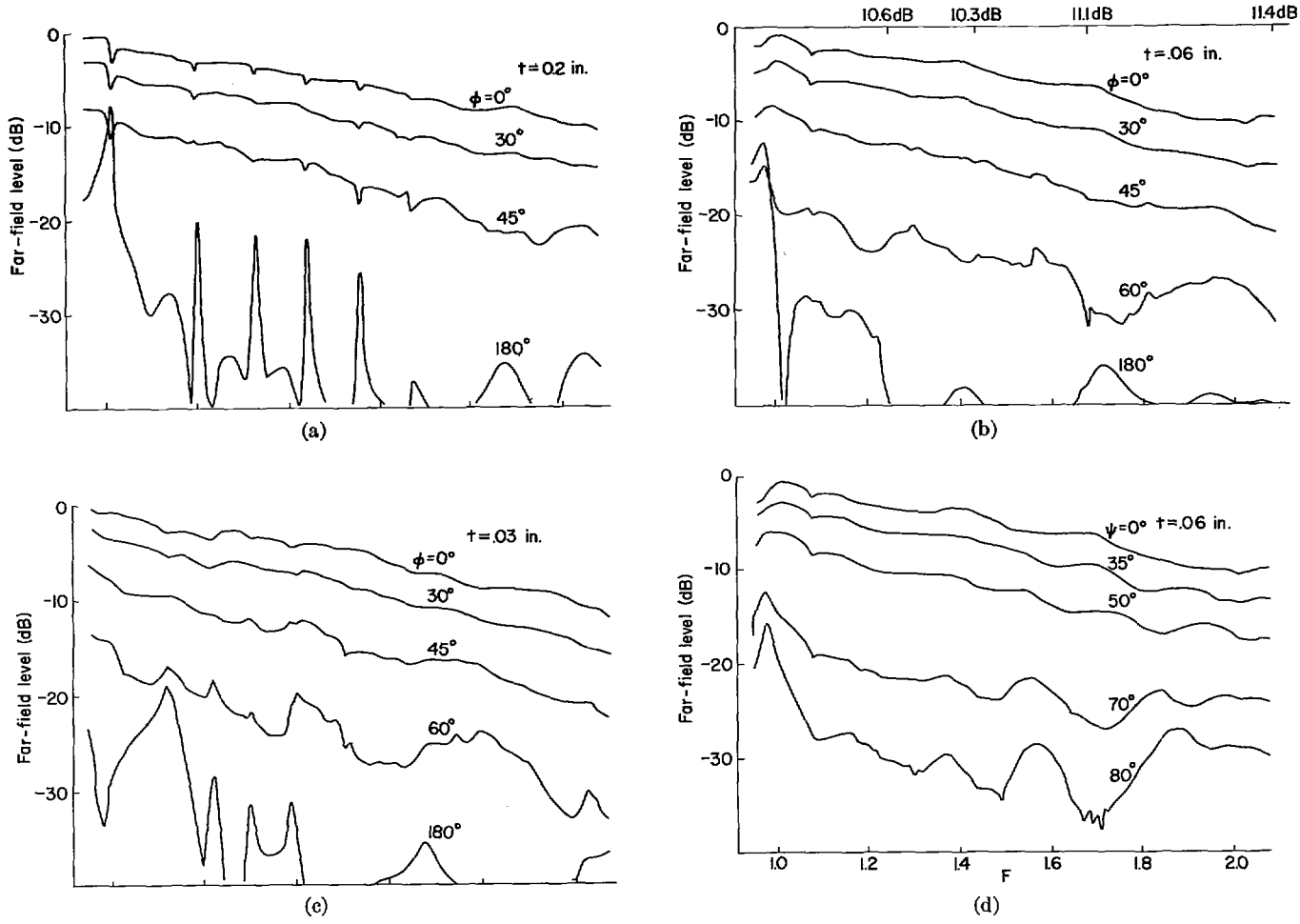

Fig. 3. Far-field swept-frequency data for $\tau = 0.94$, $\sigma = 0.1$. (a) E-plane data for $t > t_{opt}$. (b) E-plane data for $t = t_{opt}$. (c) E-plane data for $t < t_{opt}$. (d) H-plane data for $t = t_{opt}$. Directivity is given at top of (b). In all cases $\chi = 0.25$, $h_1/h_N = 3.25$.

low-reactance capacitor (to provide a short-circuit RF termination). Unfortunately the response of the diode started to roll off at about 0.62 GHz causing the experimental curves to have a slope greater than −6 dB/octave. Reflections from the chamber wall affected back-lobe level readings below about 0.6 GHz ($F = 1.2$).

At frequencies seen to be of interest from the swept data, conventional E- and H-plane radiation patterns were taken. Since at optimum t all side and back lobes are minimized, it is appropriate to calculate the directivity approximately using the formula [5]

$$G_D = 10 \log \frac{41253}{\theta_E \theta_H} \text{ dB} \qquad (1)$$

where θ_E and θ_H are the 3 dB beamwidths in the E and H planes, respectively. Fig. 2 defines the log-periodic parameters including χ (the ratio of transmission line width to radiating element length) which was chosen to be 0.25 for the experiments to be described. Initial experiments showed that values of χ somewhat less than 0.25 gave inconveniently small values of t_{opt} while appreciably larger values of χ resulted in increased side radiation.

Fig. 3 shows some of the data obtained with $\tau = 0.94$, $\sigma = 0.1$ for three values of t. For $t > t_{opt}$, Fig. 3(a) shows the anomalies as narrow bandwidth dips in the main lobe and peaks in the back radiation. They are equally spaced and are suppressed above $F = 1.6$. These are short-circuit termination measurements; with open-circuit termination the anomalies are located midway between those shown in Fig. 3(a). With a resistive termination of 400 Ω (approximately equal to the Z_0 of the transposed transmission line), these anomalies were completely suppressed. Figs. 3(b) and 3(d) show E- and H-planes measurements with $t = t_{opt}$. As the spacing was further decreased [Fig. 3(c)] the performance deteriorated due to the appearance of a different form of back radiation anomaly which was not affected by the termination.

Fig. 4 shows a set of data for $\tau = 0.94$, $\sigma = 0.15$. Note the increased directivity and low back radiation at optimum in Fig. 4(b). A very clear picture of the performance when t is less than optimum is shown in Fig. 4(c) where the anomaly frequencies appear in geometric progression with common ratio $1/\tau$. Fig. 5 shows the front-to-back and front-to-side ratios for $\tau = 0.9$, $\sigma = 0.1$. Again the optimum t is clearly seen. In Fig. 5 note that the side radiation for $t = 0.15$ in increases above the frequency where the back-lobe anomalies are suppressed ($F = 1.5$). The side radiation is not suppressed by a resistive termination and is associated with a stop-region to be dis-

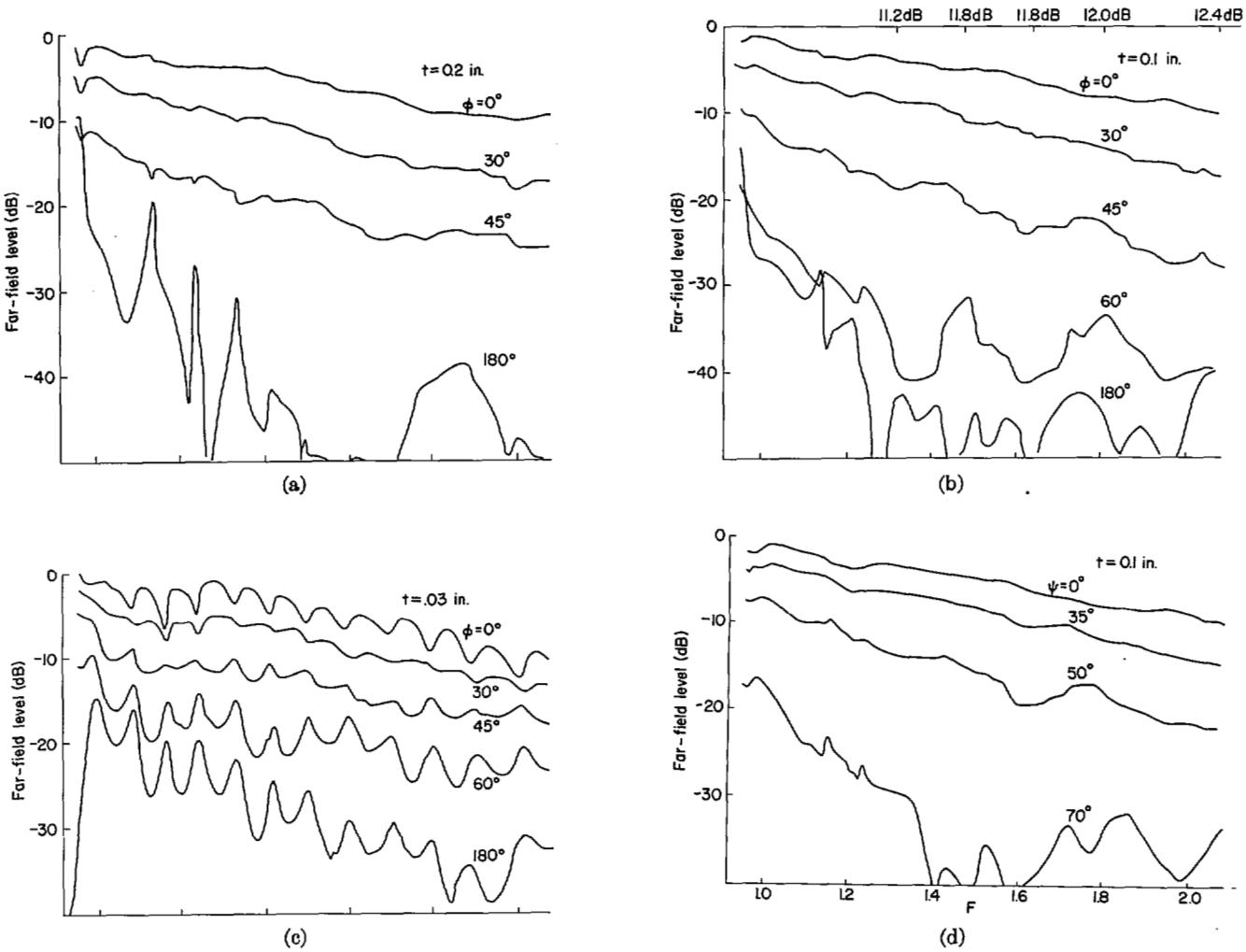

Fig. 4. Far-field swept-frequency data for $\tau = 0.94$, $\sigma = 0.15$. (a) E-plane data for $t > t_{opt}$. (b) E-plane data for $t = t_{opt}$. (c) E-plane data for $t < t_{opt}$. (d) H-plane data for $t = t_{opt}$. Directivity is given at top of (b). In all cases $\chi = 0.25$, $h_1/h_N = 3.25$.

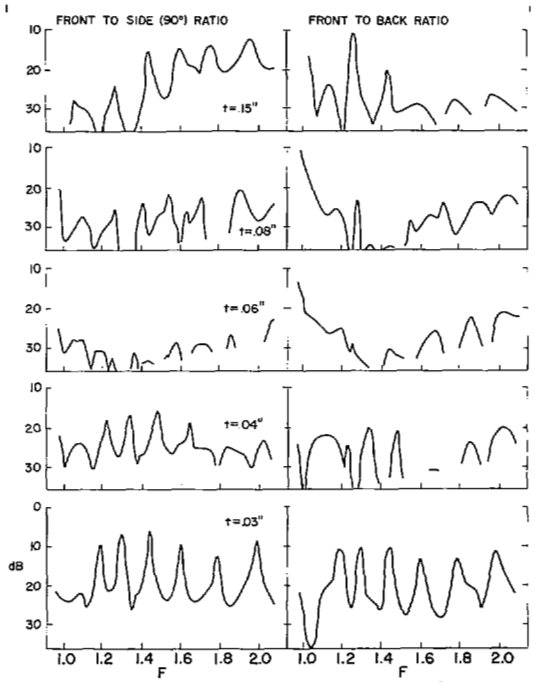

Fig. 5. E-plane front-to-side and front-to-back ratios as t is varied ($\tau = 0.9$, $\sigma = 0.1$, $\chi = 0.25$, $h_1/h_N = 2.5$).

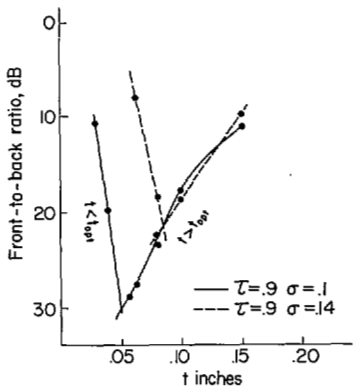

Fig. 6. Front-to-back ratio at anomaly peaks near $F = 1.26$ as t is varied ($\tau = 0.9$, $\sigma = 0.1$, $\chi = 0.25$, $h_1/h_N = 2.5$).

cussed later. The sensitivity of the optimization procedure is illustrated by Fig. 6 which shows the front-to-back ratio as a function of t near $F = 1.26$ for two antennas.

It should be noted that the form of presentation of Fig. 5 gives directivity information only and does not reveal front-lobe dips. Impedance measurement was found to be an insensitive indicator of anomalous performance.

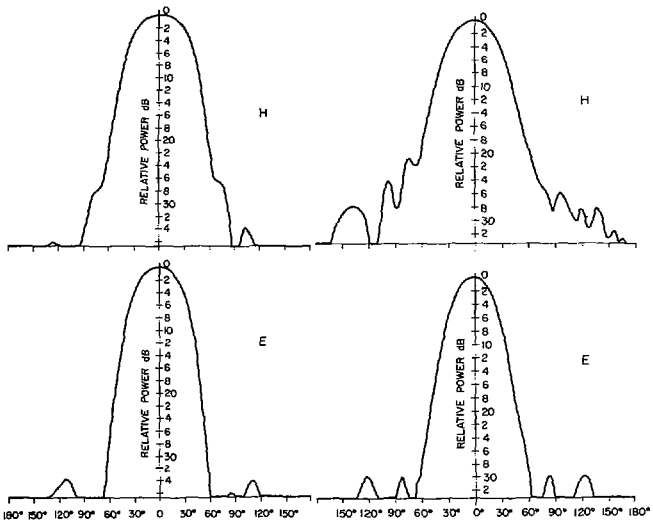

Fig. 7. Radiation patterns at two frequencies, on left $F = 1.26$, on right $F = 2.08$ ($\tau = 0.94$, $\sigma = 0.15$, $\chi = 0.25$, $t = 0.1$ in, $h_1/h_N = 3.25$).

Therefore the dips in front-lobe level are not primarily due to impedance mismatch but represent actual decreases in power gain. The best antenna tested, Fig. 4(b), had a standing-wave ratio of less than 1.4 centered on 200 Ω over the swept range. Fig. 7 shows patterns taken at both a "good" frequency as indicated by Fig. 4(b), and a "poorer" frequency at the upper end of the range. In general the directivity was found not to peak at the value of t that minimizes the anomalies but to rise about 0.2 dB for $t > t_{opt}$. It decreases rapidly for values of t less than optimum.

III. Anomalies with $t > t_{opt}$

These anomalies are similar to those found in standard LPD antennas [6] except that they occur when the half-wavelength element is at a current null on the transmission line rather than at a voltage null. The section of line behind the half-wavelength element seems to act as a resonator which is excited by a small leakage of power past the active region. If we assume that the resonator length, y in Fig. 2, is measured from the termination to the element of half-length

$$h_A = \frac{qh_1}{F} \tag{2}$$

where $q = 1$ would correspond to the half-wavelength element, the anomalies as defined occur at normalized frequencies

$$F_i = iv_p \tan \alpha + q = iv_p \frac{1 - \tau}{4\sigma} + q \tag{3}$$

where v_p is the relative phase velocity of the forward wave on the line (assumed constant) normalized to the free-space plane-wave velocity c, with $i = 1,3,5,\cdots$, for short circuit termination, and $i = 0,2,4,\cdots$, for open-circuit termination. Thus it is seen that if the experimental anomaly frequencies are plotted against the anomaly number i, the slope of the resulting line allows determination of v_p and the intercept q allows determination of the position of the front end of the resonator. The plotted results from several antennas showed that q is within a few percent of unity but that the apparent resonator length shortens slightly as t is decreased. For $t \gg t_{opt}$, v_p was found to equal the ratio of the cell length to the length of one wire in the cell (Fig. 2) which is

$$v_u = \frac{(1 + \tau)\sigma}{\tau\chi + (1 + \tau)\sigma\{1 + [\chi^2(1 - \tau)^2/16\sigma^2]\}^{1/2}}. \tag{4}$$

Thus v_u is the maximum relative phase velocity in air on the unloaded transmission line.

IV. Dispersion Diagrams

Much can be learned about the performance of two coupled structures if their individual uncoupled dispersion diagrams are known. Using an approximate technique whereby these k_0d-βd diagrams may be regarded as a plot of the phase constant along a log-periodic array [7], one can obtain useful information about phase matching in the two coupled structures comprising the loop-coupled log-periodic antenna. The k_0d-βd diagram for periodically spaced dipoles is given by [8]. The k_0d-βd diagram for a periodically transposed line is nearly the same as for an ordinary transmission line loaded with capacitors of value C_t equal to the capacitance between the wires of the transposition and whose unloaded relative phase velocity is v_u [9]. In such an infinite line the dispersion relationship is [10]

$$|\cos \beta d| = |\cos \beta_u d - \pi f C_t Z_0 \sin \beta_u d| \tag{5}$$

in which Z_0 is the characteristic impedance of the unloaded line, β is the desired phase constant of the loaded line and β_u is the phase constant of the unloaded line given by

$$\beta_u = \frac{k_0}{v_u} = \frac{2\pi f}{cv_u}. \tag{6}$$

From Fig. 2,

$$C_t = 2\chi h C_m = \frac{\chi C_m \tau d}{\sigma(1 + \tau)} \tag{7}$$

where

$$C_m = \frac{8.86P}{2t} \times 10^{-12}$$

is the distributed capacitance in F/m in the transpose where P is the transpose strip conductor width in inches. Substituting (6) and (7) into (5)

$$|\cos \beta d| = \left|\cos\left(\frac{k_0 d}{v_u}\right) - \frac{Z_0 \chi C_m \tau c k_0 d}{2\sigma(1 + \tau)} \sin\left(\frac{k_0 d}{v_u}\right)\right|. \tag{8}$$

Since d in a log-periodic structure is proportional to the distance from the apex, we can change the k_0d variable to one that gives the number of free-space wavelengths

from the apex, namely W:

$$k_0 d = \frac{\pi(1-\tau^2)W}{\tau}. \tag{9}$$

Substituting (4) and (9) into (8) gives

$$|\cos \beta d| = \left|\cos A - \frac{WC_m \pi \chi c Z_0 (1-\tau)}{2\sigma} \sin A\right| \tag{10}$$

where

$$A = \frac{W\pi(1-\tau)}{\tau\sigma}\left\{\tau\chi + (1+\tau)\sigma\left[1 + \frac{\chi^2(1-\tau)^2}{16\sigma^2}\right]^{1/2}\right\}. \tag{11}$$

The function $\beta d = f(W)$ may be plotted as shown in Fig. 8 with an additional backward mode due to the periodic transposition [7]. Certain of the experimental phenomena may be explained from this curve alone. Note that on a long enough structure a stop-region, analogous to a stop band, would start at b on the transmission line. However on the truncated antenna, the boundaries of which are shown as a function of F by the two lines to the left of the diagram, this stop-region (SR) does not exist on the structure until F exceeds F_{SR} at a. At frequencies above F_{SR}, however, the stop-region isolates the termination, thus suppressing the $t > t_{opt}$ anomalies above F_{SR} as shown in Fig. 3(a). As noted previously, under these conditions Fig. 5 shows increased side radiation; the currents in the stop region, although decaying are nevertheless in phase from cell to cell, thus tending to radiate more effectively than elsewhere on the line.

The relative phase velocity of any mode at any point on the structure in the pass region can be estimated from the slope of the line from the origin to the appropriate point on the curve:

$$v_p = \frac{\pi(1-\tau^2)}{\tau}\cdot\frac{W}{\beta d} = \frac{\pi(1-\tau^2)}{\tau} S. \tag{12}$$

For example, the phase velocity of the backward mode, which is the one that couples to the antenna elements at the transpositions, varies from a very low value at the front of the antenna to a very high value near the back which could exceed the speed of light. When the radiating element dispersion curve is superimposed on the transmission line backward wave curve (Fig. 9), it is seen that their intersection shows the position on the antenna where the modal phase velocities on each structure are equal. Since the tangents to the two curves have opposite signs, their group velocities are in opposite directions. Under these conditions a region of active coupling [11], [12] is set up (dotted lines on either side of the intersection) whose width depends on the degree of coupling present. In this region the power flowing in the forward direction down the transmission line is transferred to the antenna elements where it is guided in the backward direction and radiated. The upper edge of the active coupling region would seem to define the front boundary of the large-end resonator section mentioned in connection with the $t > t_{opt}$ anomalies.

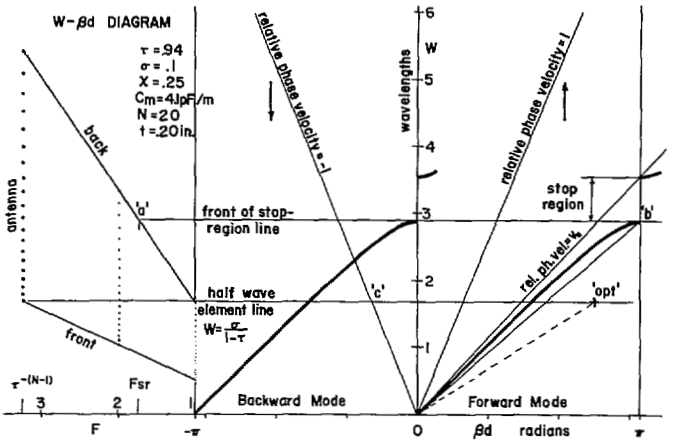

Fig. 8. W-βd diagram of transposed transmission line. Shown is phase shift βd, in rad/cell, at a distance of W free-space wavelengths from apex. The truncation locations as functions of F are shown to left ($Z_0 = 400\,\Omega$).

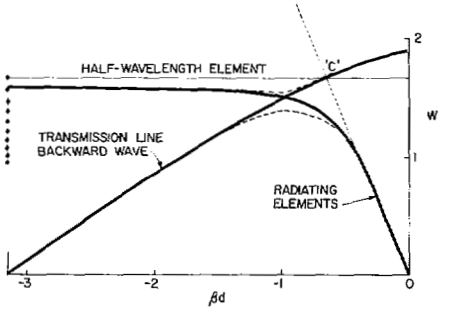

Fig. 9. Shown is intersection of W-βd curve of transposed transmission line and that of radiating elements for parameters $\tau = 0.94$, $\sigma = 0.1$, $\chi = 0.25$. Dashed lines qualitatively define relationships on combined structure for finite coupling. Dots to left show element locations for $F = 1$.

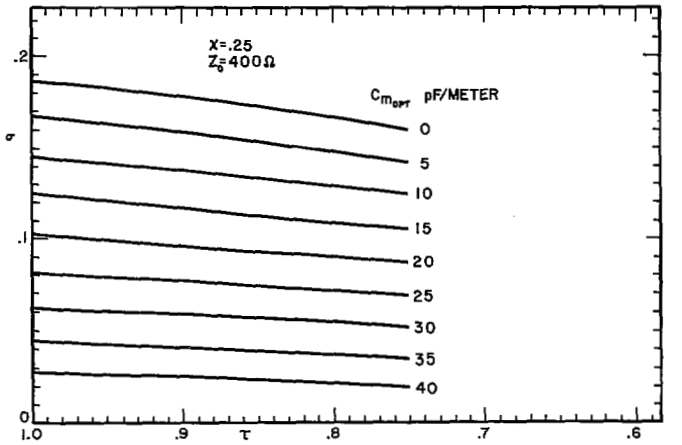

Fig. 10. Value of C_m that results in the backward-wave dispersion curve of transposed transmission line passing through point c on Fig. 8 is shown on τ-σ plane for $\chi = 0.25$ and $Z_0 = 400\,\Omega$.

It was noted using the experimental data from several antennas that the transmission line curve at optimum passed near c, the point corresponding to unity relative phase velocity at the half-wavelength element. Substitution of this point, which has coordinates

$$W_c = \frac{\sigma}{1-\tau} \qquad (\beta d)_c = -\frac{\pi\sigma(1+\tau)}{\tau} \tag{13}$$

into (10) and (11) gives the approximate value of C_m required for optimum performance. The results are plotted in Fig. 10 from which this value of C_m can be estimated for any given τ and σ, assuming the choice of $\chi = 0.25$ to be suitable.

V. Conclusions

For given suitable values of τ, σ, and χ, the anomalous performance of this antenna can be minimized and usually eliminated by adjusting the element-to-feeder spacing t. This optimization by anomaly reduction amounts to maximizing the transfer efficiency in the region of active coupling from the transmission-line mode to the required radiating-element mode.

References

[1] K. G. Balmain and S. W. Mikhail, "Loop coupling to a periodic dipole array," *Electron. Lett.*, vol. 5, no. 11, pp. 228–229, May 29, 1969.
[2] K. G. Balmain, C. C. Bantin, C. Oakes, and L. David, "Optimization of log-periodic dipole antennas," *IEEE Trans. Antennas Propagat.* (Commun.), vol. AP-19, pp. 286–288, Mar. 1971.
[3] C. R. Oakes, "Optimization of the loop-coupled log-periodic antenna," M.A.Sc. thesis, Dep. Elec. Eng., Univ. Toronto, Toronto, Ont., Canada, 1971.
[4] E. C. Jordan and K. G. Balmain, *Electromagnetic Waves and Radiating Systems*. Englewood Cliffs, N.J.: Prentice-Hall, 1968, pp. 410–412.
[5] J. D. Kraus, *Antennas*. New York: McGraw-Hill, 1950, pp. 23–26.
[6] C. C. Bantin and K. G. Balmain, "Study of compressed log-periodic dipole antennas," *IEEE Trans. Antennas Propagat.*, vol. AP-18, pp. 195–203, Mar. 1970.
[7] R. E. Collin and F. J. Zucker, *Antenna Theory, Part 2*. New York: McGraw-Hill, 1969, pp. 192–235.
[8] L. C. Shen, "Numerical analysis of wave propagation on a periodic linear array," *IEEE Trans. Antennas Propagat.* (Commun.), vol. AP-19, pp. 289–292, Mar. 1971.
[9] K. A. Roberts, "The transposed transmission line: theory and experiment," M.A.Sc. thesis, Dep. Elec. Eng., Univ. Toronto, Toronto, Ont., Canada, 1971.
[10] L. Brillouin, *Wave Propagation in Periodic Structures*. New York: Dover, 1953, pp. 218–223.
[11] W. H. Louisell, *Coupled Mode and Parametric Electronics*. New York: Wiley, 1960, pp. 30–31.
[12] J. B. Knorr, "A note on log periodically coupled modes of propagation," *Proc. IEEE* (Lett.), vol. 59, pp. 1624–1625, Nov. 1971.

Design of Multiple-Edge Blinders for Large Horn Reflector Antennas

DAVID T. THOMAS

Abstract—**Attaching blinders to the sides of pyramidal horn reflector antennas and other large aperture antennas is one method of controlling high sidelobes for horizontal polarization. This paper describes analysis and design procedures for arriving at a useful multiple-edge blinder for reducing undesirable sidelobes of a pyramidal horn reflector antenna. Several blinders have been designed and tested for use with a pyramidal horn reflector antenna. They are directed at reducing a high sidelobe near 90° in the azimuth plane where levels (referred to the main lobe) of −52 dB at 3.74 GHz and −58 dB at 6.325 GHz are presently typical. A 14-edge blinder designed using these techniques reduced these levels by 20 dB at 3.74 GHz and 12 dB at 6.325 GHz and did not significantly degrade antenna performance for other angles and other polarizations.**

I. Introduction

THE PYRAMIDAL horn reflector antenna [1] is a combination of a square electromagnetic horn and a reflector which is a sector of a paraboloid of revolution. Front and side views of this antenna with the coordinates to be used here are shown in Fig. 1. The pyramidal horn reflector antenna [1] for which the blinders are being designed has the following aperture dimensions:

Side tilt angle	$\alpha = 14.5°$.
Front tilt angle	$\beta = 15°$.
Length of side edges	$L = 2b = 2.59$ m.
Average aperture width	$W = 2.59$ m.
Width at top of aperture	3.26 m.
Width at bottom of aperture	1.92 m.

The frequency bands of operation are 3.70–4.20 GHz, 5.925–6.425 GHz, and 10.7–11.7 GHz. The antenna gain is 39.5 dB in the 4 GHz band, 43.0 dB in the 6-GHz band, and 47.5 dB in the 11-GHz band.

One very important feature of pyramidal horn reflector antennas is the very low sidelobes in much of the azimuth plane (X_0Y_0 plane in Fig. 1.) This fact is reflected in current American Telephone and Telegraph radio relay system requirements. For two routes converging on the same point, or tower, sidelobe levels 62 dB below the

Manuscript received August 1, 1972; revised October 10, 1972.
The author was with Bell Telephone Laboratories, Inc., North Andover, Mass. He is now with Raytheon Company, Goleta, Calif. 93017.